International Journal of Pure and Applied Mathematics

Volume 58 No. 4 2010, 381-416

NUMERICAL MODELING OF ONE-DIMENSIONAL BINARY SOLIDIFICATION — THE CLASSICAL TWO-PHASE STEFAN PROBLEM

Daniel Lee[1] §, D.V. Alexandrov[2]

[1]Department of Mathematics
Tunghai University
Taichung, 40704, TAIWAN, R.O.C.
e-mail: danlee@thu.edu.tw

[2]Department of Mathematical Physics
Ural State University
51, Lenin Ave., Ekaterinburg, 620083, RUSSIAN FEDERATION
e-mail: Dmitri.Alexandrov@usu.ru

Abstract: We consider in this work the heat diffusion of one-dimensional spatial variable in the semi-infinite interval. Both fixed and moving coordinates will be considered. We investigate for each model the numerical methods and discuss the issues in software design and the trade-offs between accuracy and efficiency, based on the analytic solution. In particular, we propose a threshold strategy in fixed coordinate static grid approach and show it performs very well in many tests. The observations can be helpful in practical applications of mushy layer models, for which no explicit solution is expected.

AMS Subject Classification: 65-05, 65M06
Key Words: heat transfer, solidification, Stefan problem

Received: November 18, 2009

§Correspondence author

Nomenclature

α – the Stefan constant;
Δt – the temporal meshsize in computation;
Δx – the spatial meshsize in computation;
e_{av} – normalized 1-norm of errors in calculated temperature over all spatial nodes;
e_{max} – maximum norm of errors in calculated temperature over all spatial nodes;
$e_{_S}$ – signed error in the calculated interface position;
$k_{_I}$ – thermal conductivity of the solid phase (ice);
$k_{_W}$ – thermal conductivity of the liquid phase (water);
n_t – total number of time steps in marching;
n_i – the number of computational nodes in water region at initial time;
n_f – the number of computational nodes in water region at final time;
n_x – the number of interior computational nodes in the spatial variable;
r_{av} – normalized 1-norm of the residual vector in calculation of the discrete algebraic system;
r_{max} – maximum norm of the residual vector in calculation of the discrete algebraic system;
S – one-point interface as the water-ice boundary;
t – the temporal variable in the semi-infinite interval;
T_{Ice} – constant temperature at the far-field;
T_{Water} – constant temperature at the left boundary;
$t1_{cpu}$ – the *cpu-time* in the whole time marching in solving the discrete system, excluding report on screen;
$t2_{cpu}$ – the *cpu-time* in the whole time marching, without overhead in pre- and post-processing;
u – temperature distribution in semi-infinite interval, $^{\text{O}}$C;
v – transformed image of u in finite interval, $^{\text{O}}$C;
x – spatial coordinate in models in semi-infinite interval ;
ξ – spatial coordinate in models in finite interval ;
$\xi_{_S}$ – transformed image of S in finite interval.

Subscripts

t – temporal derivatives in semi-infinite interval;
τ – temporal derivatives in finite interval;
x – spatial derivatives in semi-infinite interval;
ξ – spatial derivatives in finite interval.

1. Introduction

We consider in this work the temperature function $u = u(x,t)$, defined for temporal variable $t \geq 0$ and one-dimensional spatial variable x in the semi-infinite interval. Traditionally the study of directional solidification was and is performed within the framework of the classical model [23], leading to the Stefan boundary-value problem. However, often the plane front of solidification is broken by the constitutional supercooling arising under certain circumstances ahead of the front [15]. For this reason, some parts of the front grow in more favorable conditions than others, i.e. the front becomes morphologically unstable [18]. An evolution of such an instability leads to the appearance of a metastable zone between solid and liquid phases, which is called the two-phase zone or mushy region. Thus, after a lapse of time, solidification is divided into three parts: solid, mushy and liquid regions. The theoretical description of such a scenario of binary melt crystallization was suggested by a number of authors [13, 12, 7]. Attempts at obtaining approximate solutions were made by a number of investigators [13, 12, 7, 27, 9]. However, approximate analytical solutions were obtained by Alexandrov (see, among others, [1, 2, 3]), who analyzed the solidification of a binary melt with a mushy region, in which heterogeneous inclusions of the new phase grow in such a manner that this region is virtually totally desupercooled. Huppert and Worster [14] outline six different regimes that arise depending on whether the initial liquid concentration is less than, equal to, or greater than the eutectic composition, and whether the liquid is cooled from an upper or a lower horizontal boundary. Following the model by Worster [27], we shall investigate solidification in the absence of gravity, though this situation may almost be realized in the laboratory [14] by cooling from below, a liquid whose initial concentration is less than the eutectic value, since then the temperature and concentration fields are individually statically stable to convective turnover.

We formulate in Section 2 the classical model problem in semi-infinite interval with fixed or moving coordinates. Both one-phase and two-phase problems are explicitly stated. Numerical methods for all these models are investigated in Section 3, followed in the next section are numerical experiments and discussions. Conclusion on the relative spirits of all these numerical modelings is given in the final section.

The authors have been working on solving the real life problem [17, 26], for which no explicit solution is expected and very long time computation needed. Many decisions in the associated DNS (Direct Numerical Simulation) are made

based on observations noted from kind of burning tests in this paper. We mention that the phase field function approach (see [11, 16]) is not considered in this work since the approach we take in the currect paper is natural for an extended mushy layer model, and that in a sense the level set method (see [21, 19]) is embedded and simplified in our algorithm and software design.

2. Stefan Problem in Semi-Infinite Interval

A classical model of the application problem is in the semi-infinite interval $0 \le x < +\infty$. Since some research work focused numerically in the one-phase problem [4], we list below explicitly both the two-phase and one-phase problems, separately, for clarity and ease of reference.

2.1. Fixed Coordinate System in Semi-Infinite Interval

Model I. Semi-infinite interval $[0, +\infty)$ *with fixed coordinate system.*

Two-phase Stefan problem in semi-infinite interval:

Water zone, $0 \le x \le S(t)$

$$\text{PDE: } u_t = k_{_W} u_{xx}\,, \qquad 0 < x < S(t),\ 0 < t, \tag{2.1}$$

$$\text{B.C.: } \begin{array}{ll} u(x=0,t) = T_{\text{Water}} > 0, & 0 \le t, \\ u(x=S,t) = 0, & 0 \le t. \end{array} \tag{2.2}$$

Interface, $x = S(t)$

$$\text{ODE: } \alpha \frac{dS(t)}{dt} = k_{_I} u_x(S^+,t) - k_{_W} u_x(S^-,t), \tag{2.3}$$

$$\text{I.C.: } S(t=0) = 0. \tag{2.4}$$

Ice zone, $S(t) \le x < +\infty$,

$$\text{PDE: } u_t = k_{_I} u_{xx}\,, \qquad S(t) < x < +\infty,\ 0 < t, \tag{2.5}$$

$$\text{B.C.: } \begin{array}{ll} u(x=S(t),t) = 0, & 0 \le t, \\ u(x=+\infty,t) = T_{\text{Ice}} < 0, & 0 \le t, \end{array} \tag{2.6}$$

One-phase Stefan problem in semi-infinite interval:

Water zone, $0 \le x \le S(t)$,

$$\text{PDE: } u_t = k_{_W} u_{xx}\,, \qquad 0 < x < S(t),\ 0 < t, \tag{2.7}$$

$$\text{B.C.:} \quad \begin{array}{ll} u(x=0,t) = T_{\text{Water}} > 0, & 0 \le t, \\ u(x=S,t) = 0, & 0 \le t. \end{array} \tag{2.8}$$

Interface, $x = S(t)$,

$$\text{ODE: } \alpha \frac{dS(t)}{dt} = -k_{_W} u_x(S^-, t), \tag{2.9}$$

$$\text{I.C.: } S(t=0) = 0. \tag{2.10}$$

Ice zone, $S(t) \le x < +\infty$,

$$u(x,t) = \text{constant} = T_{\text{Ice}} = 0. \tag{2.11}$$

Analytic similarity solution to the two-phase model exists as follows [11, 25].

$$\begin{array}{rclcrcl} u_{_W}(x,t) & = & T_{\text{Water}}(1 - \frac{\text{erf}(\eta)}{\text{erf}(\frac{\alpha}{2\sqrt{k_{_W}}})}), & \eta & = & \frac{x}{2\sqrt{k_{_W}}\sqrt{t}}, \\ u_{_I}(x,t) & = & T_{\text{Ice}}(\frac{\text{erfc}(\eta)}{\text{erfc}(\frac{\alpha}{2\sqrt{k_{_I}}})} - 1), & \eta & = & \frac{x}{2\sqrt{k_{_I}}\sqrt{t}}. \end{array} \tag{2.12}$$

This includes the one-phase model as a special case. We note the interface position $S(t)$ is uniquely determined in deriving the solution. We leave details to the cited references. Plots of the solution and its temporal derivative at several specific time instances and two-hundred spatial nodes are shown in Figures C.1(a,b).

An alternative of analytic solution, subject to the Dirichlet boundary condition at the far-field and a Robin type boundary condition at the origin, is the following traveling wave solution with a one-point interface

$$\begin{array}{rcl} u_{_W}(x,t) & = & -\mu_{_W} + \mu_{_W} \exp \frac{(t-x)}{k_{_W}}, \\ u_{_I}(x,t) & = & -\mu_{_I} + \mu_{_I} \exp \frac{(t-x)}{k_{_I}}, \\ S(t) & = & t. \end{array} \tag{2.13}$$

Here the positive constants $\mu_{_I}$ and $\mu_{_W}$ satisfy a constraint

$$0 < \mu_{_I} \le 1 < \mu_{_W}$$

which implies, among other things, the positivity of the Stefan constant. A transformed system of this, in a finite interval and in one-phase version, was used as a test problem in some research [4]. However, if reformulated with Dirichlet data at both the infinity and the origin, the temperature at the origin grows unbounded in time. Aiming at obtaining relevant knowledge in solving the classical Stefan problem and further solving the real life problem [17, 26], we will not consider this (system and the) explicit solution in the sequel.

2.2. Moving Coordinate System in Semi-Infinite Interval

Consider the time-dependent coordinate transform and its inversion

$$\xi = \xi(x,t) = \frac{x}{S(t)}, \quad x = \xi S(t).$$

This maps the triple $x \in \{0, S, +\infty\}$ to $\xi \in \{0, 1, +\infty\}$, and $\{0, S, MS\}$ to $\{0, 1, M\}$ with M a sufficiently large integer for computational purpose.

The relation $u(x,t) = v(\xi,\tau)$ with $\tau = t$ and ξ as defined above implies, by application of chain rule,

$$u_t = v_\tau + \xi_t v_\xi, \quad u_x = \xi_x v_\xi, \quad u_{xx} = (\xi_x)^2 v_{\xi\xi} + \xi_{xx} v_\xi.$$

These, together with the substitution that,

$$\xi_t = \frac{-\xi S'(t)}{S(t)}, \quad \xi_x = \frac{1}{S(t)}, \quad \xi_{xx} = 0,$$

yield a transformed system in terms of $v(\xi,\tau)$. A final formal replacement gives following system, still in $u(x,t)$.

Model II. Semi-infinite interval $[0, +\infty)$ *with moving coordinate system.*

Two-phase Stefan problem in semi-infinite interval:

Water zone, $0 \le x \le 1$,

$$\text{PDE: } S^2(t)u_t = k_{_W} u_{xx} + xS(t)\frac{dS(t)}{dt}u_x, \quad 0 < x < 1,\ 0 < t, \tag{2.14}$$

$$\text{B.C.: } \begin{array}{ll} u(x=0,t) = T_{\text{Water}} > 0\,, & 0 \le t, \\ u(x=1,t) = 0\,, & 0 \le t. \end{array} \tag{2.15}$$

Interface, $x = 1$,

$$\text{ODE: } \alpha S(t)\frac{dS(t)}{dt} = k_{_I} u_x(1^+,t) - k_{_W} u_x(1^-,t), \tag{2.16}$$

$$\text{I.C.: } S(t=0) = 0. \tag{2.17}$$

Ice zone, $1 \le x < +\infty$,

$$\text{PDE: } S^2(t)u_t = k_{_I} u_{xx} + xS(t)\frac{dS(t)}{dt}u_x, \quad 1 < x < +\infty,\ 0 < t, \tag{2.18}$$

$$\text{B.C.: } \begin{array}{ll} u(x=1,t) = 0\,, & 0 \le t, \\ u(x=+\infty,t) = T_{\text{Ice}} < 0\,, & 0 \le t. \end{array} \tag{2.19}$$

One-phase Stefan problem in semi-infinite interval:

Water zone, $0 \le x \le 1$,

$$\text{PDE: } S^2(t)u_t = k_{_W} u_{xx} + xS(t)\frac{dS(t)}{dt}u_x, \quad 0 < x < 1,\ 0 < t, \tag{2.20}$$

$$\text{B.C.: } \begin{array}{ll} u(x=0,t) = T_{\text{Water}} > 0, & 0 \le t, \\ u(x=1,t) = 0, & 0 \le t. \end{array} \tag{2.21}$$

Interface, $x = 1$,

$$\text{ODE: } \alpha S(t)\frac{dS(t)}{dt} = -k_{_W} u_x(1^-, t), \tag{2.22}$$

$$\text{I.C.: } S(t=0) = 0. \tag{2.23}$$

Ice zone, $1 \le x < +\infty$,

$$u(x,t) = \text{constant} = T_{\text{Ice}} = 0. \tag{2.24}$$

A spatial transformation is applied in Appendix A to yield Stefan problems on the finite interval $[-1, 1]$ in fixed coordinate.

3. Numerical Methods and Software Issues

The application problem consists of three subsystems:

1. The solid (ice) zone, with PDE and B.C. depending on a moving boundary.

2. The solid-liquid interface, with ODE describing the interface dynamics.

3. The liquid (water) zone, with PDE and B.C. depending on a moving boundary.

The idea of shooting for one-dimensional (nonlinear) boundary value problems, by solving iteratively an initial value problem, is adopted here. However, no variational technique is implemented for the outer loop due to the complications and expensive cost in cpu-time of a fully implicit approach in possible multi-dimensional extensions of our work. Details of the method are described below.

One way to tackle the application in semi-infinite interval is to truncate the domain to a finite interval somehow appropriately. This is what we did (Table B.3) and will be explained in a later subsection when discussing numerical experiments. With computational domain being a finite interval, the methods described below are applied to systems of equations in all models previously discussed.

Two-level finite difference is applied to the temporal derivative. For spatial derivatives, finite difference (FD) or differentiation matrix (DM) approach (see [8], [10], [22]) is taken. Central differences are applied in the former case. Spatial differentiations for subsystems in the solid or liquid zone can be implicit or explicit. In the implicit FD approach, the resulting discrete algebraic (sub)systems are solved by three-point stencil GS (prefered over SOR for better consistence) with various types of node ordering, and also by tri-diagonal Gaussian elimination (GE) as a double check for some test runs. The discrete subsystems in the spatial spectral approach, involving the Chebyshev differentiation matrix, are solved by dense LU and dense *BCGstab* [20] as a double check for some tests.

More details follow.

Discretization of the Geometry. The coordinate systems can be either of the following:

1. Fixed coordinate grid.

Within this group, we can further consider:

— Static Grid: A single grid is deployed here. It is uniform in the FD approach, while in the DM approach Chebyshev nodes are chosen.

— Dynamic Grid: Time dependent grid. This is sub-uniform in the FD approach, uniform in both water and ice zones with probably different mesh sizes. In the DM approach, the numbers of Chebyshev nodes in water and ice regions may (or need to) be adjusted as the interface moves in time.

2. Moving coordinate grid.

Here the one-point interface is always an integral node. The number of nodes to the left, the water zone, is kept a constant in a straight-forward implementation in the FD approach. The methods and software design with a moving grid are complicated issues and we refer to [24] for further discussion.

Some of the resulting effects in our algorithmic design are noted below, with more discussions and observations on experimental tests later.

1. The fixed static grid approach was regarded as unstable in the literature [11]. We designed a threshold strategy as an improvement. This works very well in the current problem, and also works for a mush-layer model in a real-life problem.

2. The dynamic fixed coordinate grid is very costly and the (cubic) spline interpolation, although quite stable, cannot keep up with the high precision obtained in nonlinear iterations. It is expected, in this situation, that Hermite

splines may perform better, although not easily extendable to higher dimensional Stefan problems.

3. The moving grid approach, for a two-phase problem, seems inferior to all the above in both accuracy and efficiency. This may be due to the generic difficulty that the water zone is small in size compared to the ice zone, in all tests of our applications.

Discretization of the Equations. Two-level FD scheme is applied to the temporal variable. Options are:

— Explicit forward Euler scheme,

— Implicit backward Euler scheme.

We note that MOL type approach for temporal discretization is a popular method for the moving grid, at least easy for one-phase problem. But it is impractical for (static or dynamic) fixed grid approache to the two-phase problems because of computational inefficiency due to the moving interface.

The spatial derivatives are resolved through either of the following:

— Finite Differencing

Second order central in the diffusion term in both water and ice zones, and one-sided approximation optionally in various orders for the interface dynamics (the Stefan condition). We note that Gauss-Seidel type (nonlinear) functional iteration, other than Jacobi one, is preferred for the coupled system. The reported on-screen statistics about the iteration counts and the resulting residuals show infomation in the convergence status about strength of the nonlinearities. Although, tri-diagonal version of LU works slightly more efficient as an optional double check.

— Spectral Collocation via Differentiation Matrices

Chebyshev nodes are taken and dense-version LU and *BCGstab* methods serve as linear solver in each nonlinear procedure.

Other Numerical Issues in FD-FD Approach. Here we discuss several things which may be important to practictioners.

— extrapolation

When solving the interface dynamics, we need one-sided derivatives in the Stefan condition at the interface. Various one-sided schemes are designed for this purpose. These include:

— Scheme 1: two-point first-order finite difference approximation.

— Scheme 2: three-point second-order finite difference extrapolation.

— Scheme 3: four-point third-order finite difference extrapolation.

— Schemes 5, 6, 7: Crank-Nicolson type variants of the above three schemes.

— Others: exponential type extrapolation scheme.

Our numerical experiment suggests usage of the four-point scheme for accuracy as shown in Table B.4. The Crank-Nicolson type variants are not worthy of the (doubled) efforts.

— interpolation.
In the moving and the dynamic fixed grid approaches, interpolations are needed at the end of each time step. Among various options, the natural and the not-a-knot cubic spline interpolations are designed for the current second order PDE system. The latter are fourth-order accurate in theory as proved by de Boor [5, 6]. Although, we found no significant difference in choosing either of the spline interpolants in long time simulation, with the (fine) spatial meshes we deployed.

— threshold strategy for the static grid.
In the fixed coordinate approach, the application of a static grid is much more difficult and complicated than that of a dynamic grid. When the interface front approaches an integral computational node, the regular three-point finite difference approximation becomes close to singular and is sensitive to truncation error. This inevitably leads to the loss of significant digits. The propagation of error can be fatal in a task of long time simulation. To overcome this intrinsic difficulty, we designed a threshold strategy in which a frontal position, when approaching a computational node and getting close within a threshold, is reassigned forward and cross the integral node appropriately, in the direction of current frontal velocity. Housekeepings are carried out accordingly, i.e., all relevant variables including the clock time are modified properly in a time march. This may yield, at the time step, a linearly compatible continuation of the physical process, provided that the threshold is roughly at the scale of the motion at one computational time step. We note the threshold we used in all results shown later is *1.0e-06* relative to the spatial mesh size. In a sense, the threshold signifies the level of relative error.

Other Numerical Issues in FD-DM Approach. We note in the FD-DM approach, the dense spectral differentiation matrix works well for grid of moderate size.

A Recursive Relation. For our test problem with analytic solution (equation (2.12)), the interface coordinate is proportional to square root of the temporal variable, or equivalently, square of the interface coordinate is linear in time. This yields a three-term recursion, which can be used as a quality check

in computation, that we did, and also as a prediction, that we found not accurate enough to be valuable in our DNS computation.

Numerical Justification via Convergence of Residuals. Our implementation of both the FTCS (Forward in Time and Central in Space) and the BTCS (Backward in Time and Central in Space) numerical schemes are about second order in the convergence of residuals as predicted in theory, for the moving grid and dynamic fixed coordinate grid cases, as shown in Tables B.5, B.6 and B.7. Although, the convergence in the errors behaves like such only for appropriate combinations of the spatial and temporal resolutions, probably because of saturation of accuracy.

4. Numerical Experiments and Discussion

4.1. Computer Environment

All numerical experiments, with *cpu-time* recorded in this paper, are running on a Tyan VX50B4985-E server system with AMD Opteron 8350 CPU at 2.0 Ghz. Other experiments without *cpu-time* statistics, are running on a Tyan server of previous generation. The software is designed in the *C-language* and compiled by *gcc* with *O2* optimization. The run time environment is practically single user and single task via remote *shell*.

4.2. Numerical Models

Test results are obtained with static or dynamic fixed coordinate grid, and also moving grid, as indicated in Table B.1. Actually, some more numerical models are tested and regarded as being inferior and therefore not included in the list. The classification of these *numerical* models is aiming at an integrated software design, and differs from the numbering of PDE systems discussed in Sections 2.

4.3. Parameters in Test Runs

Since all one-phase models are special cases of the corresponding two-phase models, with the far-field temperature set equal to zero (the freezing temperature), we report here only results of two-phase models.

Listed in Table B.2 are two sets of defaulted parameters used in all numerical

experiments reported in this paper. These include the diffusivity constants, k_W and k_I of water and ice region respectively, the Stefan constant α, and boundary temperatures. These nondimensional constants are chosen for no particular reasons. On the other hand, in computations for models in the semi-infinite interval, specific temporal and spatial ranges for each parameter set are chosen based on observations shown in Table B.3. Using the first set of parameters, the Dirichlet data in the truncated finite interval matches that in the semi-infinite domain in about 5 digits with spatial range $[0, 10]$ and 16 digits with range $[0, 20]$, and also 16 digits with range $[0, 6]$ using the second set of parameters.

Not-a-knot cubic splines are used for interpolants. It is the four-point third order extrapolation scheme that we adopted at the interface frontals. The decision is made as explained in next subsection.

The above are defaults for all tests, if not stated otherwise.

4.4. Experiments and Observations

We describe below our experiments, the resulting tables and figures, and some at-a-glance observations. More observations are noted in the next subsection.

4.4.1. Numerical Treatment in Flux Cross the Moving Boundary

Numerical procedure in the treatment of the moving boundary is critical in long time simulation. We report test on this in Table B.4. It can be concluded that, to resolve the interface dynamics, the four-point third order extrapolation to the primitive variable is the most accurate. We mention that the idea of fitting by exponential (decay) is tested but the result is not as good as that of the FD scheme presented here. Super-exponential fitting might help, probably in very high spatial resolution.

4.4.2. Five Groups of Tests

These are described below with first set of parameters. The results are summarized in Table B.5, which consists of five groups of tests corresponding to numerical models 1a, 1b, 1c, 1d and 2 as described in Table B.1. Results of mixing of schemes in the two tables are not promising. The initial and the final time for all tests are 2.0 and 12.0, respectively. The computational spatial domains is $[0, 10]$ for all tests reported here. Indicated in columns labeled by n_i

and n_f are the numbers of spatial nodes in the interior of the water region at the initial and final time, respectively. Compared with the analytic solution (equation (2.12)), errors in the calculated solution at the final time and at all spatial nodes, are reported in discrete $max-$ and normalized $1-norm$ in the e_{max} and e_{av} columns. The error in the calculated interface coordinate appears in the $e_{_S}$ column. The accumulated *cpu-time* spent within the whole time marching, with overhead in pre- and post-processing, is shown in the $t2_{cpu}$ column, and the $t1_{cpu}$ column for only solving the coupled discrete system. Convergence history, in the residuals and errors, and the preserving of the recursions, are shown in Figures C.2-6.

We note the numerical far-field boundary temperature we used is accurate in 5 digits only (Table B.3), to mimic the situations of possible applications.

More details follow.

— Within the first three groups in Table B.5, the spatial mesh is refined three times by halving, while the corresponding temporal mesh size decreases at a ratio of a quarter. The *cpu-time* spent in the time march, with or without overhead, increases roughly eight times each run as expected. Except for results on the finest grid (fourth row data of each group), which show saturation of accuracy, both the maximal and averaged errors in the calculated results decrease as of second order for model 1b (the second group). It performs better than second order with model 1a (the first group). Actually model 1a is the winner in all respects, most accurate and most economic in *cpu-time* spent. Model 1b ranked the second while model 1c the third, in both accuracy and efficiency. We note the signed-error in the calculated interface position, shown in the $e_{_S}$ column, behaves also as second order.

— The mixings of implicit and explicit solves on dynamic grid perform only slightly different than the strict explicit solve, and are much inferior to implicit solve on dynamic grid and also the static grid computation. It makes very little difference, in one step of time march, whether the interface dynamics is solved firstly (mix-1 data in table), or lastly (mix-2 data).

— The moving grid approach, as the second last group in the table, seems not appropriate for our problem. This may be due to the fact that, at the start time, the interface position is very close to the left boundary while the truncated numerical right boundary is relatively far away. Nonlinear differential equations (equations (2.14), (2.16), (2.18)) are coupled here, in contrast to the previous groups in the table, in which linear diffusions (equations (2.1), (2.5)) present in two subsystems. We mention that explicit spatial differentiation works better than the implicit one in the moving grid approach with results not shown.

— The last group in Table B.5 is concerned about the spectral collocation for dynamic grid in the semi-infinite interval, using dense *BCGstab* (first run) and *LU* (second run) as linear solver, respectively. While achieving at about the same accuracy, the computation costs more *cpu-time* in the former. It is apparent that, for current problem in the semi-infinite interval, the Chebyshev DM approach is not efficient as the FD method.

— More on history of convergence are shown in Figures C.2-6. These help to shed light on the relative spirits among the five numerical models. Implicit computations on static and dynamic grids are compared with results shown in Figures C.2 and C.3. The calculated moving interface coordinates are smooth for both model 1a (static implicit) and 1b (dynamic implicit), as shown in Figures C.2(a) and C.3(a) respectively. The derived melt speed is visually smooth in static grid (Figures C.2(b)) but not in dynamic grid (Figures C.3(b)). This indicates that too many interpolations are performed in the dynamic grid approach to keep derived physics (the melt speed) physically correct in long time simulation. Maximal and averaged residuals are shown in Figures C.2(c) and C.3(c). Errors in the calculated interface coordinates, maximal and averaged errors in the calculated temperatures are shown in Figures C.2(d) and C.3(d). The residuals and errors are about one or two magnitudes smaller in the static grid than dynamic grid. Same with the recursive relation of the moving interface (Figures C.2(e) and C.3(e). More comparison of models 1a, 1b, 1c and 1d is shown in Figures C.4, which confirms that static grid is indeed the winner, while dynamic implicit grid the second and moving grid the least desired. Here maximal and averaged residuals are shown for the corresponding models in Figures C.4(a,c,e,g). Errors in the calculated interface, maximal and averaged errors in the calculated temperature are shown in Figures C.4(b, d, f, h). The moving grid model does exhibit smoothest convergence in the recursions (Figures C.5), while the static grid the fastest convergence. The numerical behavior of model 2, the FD-DM approach, is shown in Figures C.6 with not so good accuracy. From these (sub)figures, we see that errors accumulate very soon for both the moving grid (model 1d) and the spectral nodes (model 2).

4.4.3. The First Parameter Set with 16-Digit-Accurate B.C.

For comparison, we re-run most tests for some models from above with a wider spatial range, $[0, 20]$, while keeping the same temporal and spatial mesh sizes. The results are shown in Table B.6. Compared with the case of 5-digit-accurate B.C. (Table B.5), the calculated errors in the interface and the maximal errors

in the calculated solution at the final time remain about the same (the e_S and the e_{max} column), while the averaged error reduces more than fifty-percent. Relative spirits between the static and dynamic grids remain the same as in Table B.5. The fixed static grid approach, with our threshold strategy, is both the most accurate and most efficient. The second favorable is the fixed coordinate with dynamic grid and implicit PDE solves. To make certain about this, we try different constants of physical properties next.

4.4.4. The Second Parameter Set

We test more on four numerical models, 1a, 1b, 1c and 1d. The results are shown in Table B.7 and Figures C.7. With the second parameter set being used, the numerical far-field temperature as part of the boundary condition is accurate up to 16 digits as shown in Table B.3. We note the following:

— These four numerical models behave qualitatively the same as in Table B.5, except that numerical model 1c runs very well with now truly accurate boundary data. Model 1c, dynamic grid with explicit solve, is therefore regarded not stable as the dynamic implicit and the static implicit models. The latter two can live up well with as moderate as 5-digit accurate input data (Table B.5).

— We mention that, for computation on static grid with threshold strategy, the result with explicit scheme is unstable and not shown. That with moving grid is not promising and not shown either.

4.4.5. Convergence in FD-FD Approach

Justification of our implementation in terms of residuals in calculation can be seen in Tables B.5, B.6, and B.7. We conclude that both the FTCS and BTCS finite difference schemes for the coupled nonlinear system, in our software design, are about second order accurate in spite of an internal moving boundary.

4.4.6. Second Order Extrapolation in the Semi-Infinite Interval

The story here, shown in Table B.8, is quite similar to the third order extrapolation used in Table B.5. But here the convergence in error is slightly inferior to second order, while it is superior previously.

4.4.7. The Recursion

For models in the semi-infinite interval, the interface coordinates satisfy a three-term recursion. We might therefore predict it by simple extrapolation and a predictor-corrector type fast algorithm might be thus derived. However, preliminary experiments showed unsatisfactory results along this line. On the other hand, the expected relation can be used simply as a check. The calculated interface coordinates do satisfy the three-term recursion in discrete uniform time-steping, in very high precision, as shown in the chk_S column in tables. This suggests a fact that in direct numerical simulation a perturbed system is being solved with truncation errors decay in time. Recall the qualitative and quantitive behaviors in computation on static and dynamic grid, Figures C.2 and C.3 the recursions are kept numerically on both grids, with results Figures C.2(e) and C.3(e) showing advantages in static grid.

4.5. Observations

Refering to the numerical models and experiments discussed in previous subsections, we summarize below all observations.

1. Problem domains, grid arrangements and equation discretizations.

— Semi-infinite interval in fixed coordinate with FD-FD approach.

— Numerical models: 1a, 1b, 1c.

— Advantages.

Linear PDE of diffusion process. Slightly nonlinear coupling through the interface dynamics. Easily solved by efficient tridiagonal GE or 3-point stencil GS linear solve. Error propagation is not a serious problem.

— Disadvantages.

Need relatively large spatial domain for reasonably accurate boundary condition. And therefore need more grid points, which in turn calls for much finer time steps.

— Conclusion.

Very accurate and stable, at the cost of relatively more spatial nodes and long time computation.

— Semi-infinite interval in moving coordinate with FD-FD approach.

— Numerical model: 1d.

— Facts.

Application of the moving grid in the current situation encounters an intrinsic improper grid distribution. Adaptive grid methods may be needed [24].

— Semi-infinite interval in fixed coordinate dynamic grid with FD-DM approach.

— Numerical model: 2.

— Facts.

(1) Finer mesh is needed if the start time t_0 is too close to 0. In such a case, initial x_S can be as small as 0.2, therefore small spatial mesh size is needed, posing difficulty to the application of both (sub-)uniform mesh and Chebyshev nodes. With such, the situation with Chebyshev nodes in the FD-DM approach is much severer than that with FD-FD on sub-uniform mesh.

(2) More nodes are needed towards the infinity to reasonably represent the boundary value at the truncated spatial interval. For not so small initial time, the final time will be relatively large and demands large computational domain for which numerical boundary temperature is reasonably close to the far-field temperature.

(3) There is a trade-off bewteen the above. It is difficult to satisfy both.

— Advantages.

The spectral approach needs relatively coarse spatial grid and time steps, compared to the FD-FD approach. Dense versions of both LU and *BCGstab* work well.

— Disadvantages.

Still the cost in computation time grows rapidly with refinements in spatial resolution.

— Conclusion.

Can achieve moderate accuracy at moderate cost. But may be impractical for application in which initial condition involves very small interface coordinate and relative large computational spatial domain.

2. Numerical solve.

— The implicit spatial FD method works for both dynamic and static grid. It is more stable than explicit one in solving heat conduction in either solid or liquid region. The interface ODE is resolved by Euler method, with third order extrapolation for primitive variable, in semi-infinite interval. We mention without showing numbers that second order extrapolation is prefered in finite interval models.

— The explicit spatial FD method works for moving grid better than im-

plicit one, but only in very short time.

5. Conclusion

In summary,

— The static grid approach, with the proposed threshold strategy and implicit algebraic solve, provides the most accurate results among all models in semi-infinite interval. Using the third order extrapolation scheme is helpful for this purpose.

— The dynamic grid approach is accurate and stable. Implicit algebraic solve is prefered in general. Although, explicit solve achieves better accuracy in some cases.

— As for time-dependent coordinate, the moving grid approach, the coupled system is nonlinear and advection-dominant in some spatial subdomain. However, explicit scheme with upwind FD for advection term shows very smooth convergence. A critical issue for current application is about the grid distribution.

— At the time of writing this paper, we have made successful simulations for a mushy layer model, (only) by the fixed coordinate static grid approach with the threshold strategy.

Acknowledgments

The authors thank the Tunghai University for laboratory support in a long period of time. The second author thanks the following grants and programs for the financial support: Nos. 09-08-00844, 10-01-96045 Ural (Russian Foundation for Basic Research) and 2.1.1/2571 (Ministry of Education).

References

[1] D.V. Alexandrov, Solidification with a quasiequilibrium two-phase zone, *Acta Mater.*, **49** (2001), 759-764.

[2] D.V. Alexandrov, D.L. Aseev, I.G. Nizovtseva, H.-N. Huang, D. Lee, Nonlinear dynamics of directional solidification with a mushy layer. Analytic

solutions of the problem, *Int. J. Heat and Mass Transfer*, **50** (2007), 3616-3623.

[3] D.V. Alexandrov, Nonlinear dynamics of solidification in three-component systems, *Doklady Physics*, **53**, No. 9 (2008), 471-475.

[4] Whye-Teong Ang, A numerical method based on integro-differential formulation for solving a one-dimensional Stefan problem, *Numerical Methods for Partial Differential Equations*, **24** (2008), 939-949.

[5] Carl de Boor, *A Practical Guide to Splines*, Revised Edition, Springer-Verlag, New York (2001).

[6] Carl de Boor, Convergence of cubic spline interpolation with the not-a-knot condition, In: *MRC 2876*, University of Wisconsin at Madison (1985).

[7] V.T. Borisov, *Theory of the Two-Phase Zone of a Metal Ingot*, Moscow, Metallurgiya Publishing House (1987).

[8] J.P. Boyd, *Chebyshev and Fourier-Spectral Methods*, Second Edition, Dover, Mineola, New York (2001).

[9] Yu.A. Buyevich, D.V. Alexandrov, V.V. Mansurov, *Macrokinetics of Crystallization*, Begell House, New York-Wallingford (2001).

[10] C. Canuto, M.Y. Hussaini, A. Quarteroni, T.A. Zang, *Spectral Methods, Fundamentals in Single Domains*, Springer, New York (2006).

[11] J. Crank, *Free and Moving Boundary Problems*, Clarendon Press, Oxford, England (1984).

[12] A.C. Fowler, The formation of freckles in binary alloys, *IMA J. Appl. Math.*, **35** (1985), 159-174.

[13] R.N. Hills, D.E. Loper, P.H. Roberts, A thermodynamically consistent model of a mushy zone, *Quarterly Jnl. of Mechanics and App. Maths.*, **36** (1983), 505-540.

[14] E.H. Huppert, M.G. Worster, Dynamic solidification of a binary melt, *Nature*, **314** (1985), 703-707.

[15] G.P. Ivantsov, Diffusive supercooling in binary alloy solidification, *Dokl. Akad. Nauk SSSR*, **81** (1951), 179-182.

[16] E. Javierre, C. Vuik, F.J. Vermolen, S. van der Zwaag, A comparison of numerical models for one-dimensional Stefan problem, *JCAM*, **192** (2006), 445-459.

[17] J. Morison, M. McPhee, R. Muench, et al, The LeadEx experiment, *EOS. Trans. AGU*, **74** (1993), 393-397.

[18] W.W. Mullins, R.F. Sekerka, Stability of a planar interface during solidification of a dilute binary alloy, *J. Appl. Phys.*, **35** (1964), 444451.

[19] S. Osher, R.Fedkiw, *Level Set Methods and Dynamic Implicit Surfaces*, Springer, New York (2003).

[20] Y. Saad, *Iterative Methods for Sparse Linear System*, Second Edition, SIAM, Philadelphia, USA (2003).

[21] J.A. Sethian, *Level Set Methods and Fast Marching Methods*, Cambridge University Press, New York (1999).

[22] Jie Shen, Tao Tang, *Spectral and High-Order Methods with Applications* Science Press, Beijing, P.R. China (2006).

[23] I. Stefan, Übereinige Probleme der Theorie der Warmeleitung, In: *Sitzber. Kais. Akad. Wiss. Wien, Math.-Naturw. Kl.*, **98**, No. 11a (1898), 437438.

[24] Tao Tang, Jinchao Xu, *Adaptive Computations: Theory with Algorithms*, Science Press, Beijing, P.R. China (2007).

[25] C. Vuik, Some historical notes about the Stefan problem, *Nieuw Archief voor Wiskunde*, **4e**, Serie 11 (1993), 157.

[26] J.S. Wettlaufer, M.G. Worster, H.E. Huppert, Solidification of leads: Theory, experiment and field observations, *J. Geophys. Res.*, **105** (2000), 1123-1134.

[27] M.G. Worster, Solidification of an alloy from a cooled boundary, *J. Fluid Mech.*, **167** (1988), 481-501.

Appendiax A: Stefan Problem in Finite Interval

The Stefan problem can be formulated in a finite interval as well. Considered here are a coordinate transform and its inversion

$$\xi = \xi(x)\,, \quad x = x(\xi),$$

where x denotes spatial variable in semi-infinite interval $[0, +\infty)$ and ξ in the finite interval $[-1, 1)$.

The relation $v(\xi, t) = u(x, t)$ and application of chain rule yields

$$u_t = v_t, \quad u_x = \xi_x v_\xi, \quad u_{xx} = (\xi_x)^2 v_{\xi\xi} + \xi_{xx} v_\xi.$$

One such coordinate transform will be discussed in the sequel.

A.1. Fixed Coordinate System in Finite Interval

With a real positive parameter, $x_{\rm ref}$, we consider the algebraic transformation and its inversion

$$\begin{aligned} \xi(x) &= 1 - \frac{2x_{\rm ref}}{x + x_{\rm ref}} = \frac{x - x_{ref}}{x + x_{\rm ref}} \\ x(\xi) &= x_{\rm ref}\frac{1+\xi}{1-\xi}. \end{aligned}$$

This maps the triple $x \in \{0, x_{\rm ref}, +\infty\}$ to $\xi \in \{-1, 0, 1\}$.

We note that for a uniform grid in the finite interval $[-1, 1]$ with mesh size $\varepsilon = \frac{2}{n}$, the right-most interior node, $\xi = 1 - \varepsilon$, corresponds to $x = (n-1)x_{\rm ref}$ in the semi-infinite interval.

Similar to the derivation of model II, consider the relation $v(\xi, t) = u(x, t)$ and note that

$$u_x = \frac{(1-\xi)^2}{2x_{\rm ref}} v_\xi, \quad u_{xx} = \frac{(1-\xi)^4}{4x_{\rm ref}^2} v_{\xi\xi} - \frac{(1-\xi)^3}{2x_{\rm ref}^2} v_\xi.$$

We are thus led to the following transformed problem.

Model III. Finite interval $[-1, 1]$ *with fixed coordinate system*

Water zone: $-1 \le \xi \le \xi_S$,

$$\text{PDE: } v_t = k_W \left[\frac{(1-\xi)^4}{4x_{\rm ref}^2} v_{\xi\xi} - \frac{(1-\xi)^3}{2x_{\rm ref}^2} v_\xi \right], \ -1 < \xi < \xi_S, \ 0 < t, \quad \text{(A.1)}$$

$$\text{B.C.:} \quad \begin{array}{l} v(\xi = -1, t) = T_{\text{Water}} > 0\,,\ 0 \le t, \\ v(\xi = \xi_S, t) = 0\,,\ 0 \le t, \end{array} \tag{A.2}$$

Interface: $\xi = \xi_S$,

$$\text{ODE:} \quad \alpha x_{\text{ref}} \frac{dS(t)}{dt} = k_I \frac{(1-\xi)^2}{2x_{\text{ref}}} v_\xi(\xi_S^+) - k_W \frac{(1-\xi)^2}{2x_{\text{ref}}} v_\xi(\xi_S^-) \tag{A.3}$$

$$\text{I.C.:} \quad \xi_S(t=0) = -1 \tag{A.4}$$

Ice zone: $\xi_S \le \xi < 1$,

$$\text{PDE:} \quad v_t = k_I \left[\frac{(1-\xi)^4}{4x_{\text{ref}}^2} v_{\xi\xi} - \frac{(1-\xi)^3}{2x_{\text{ref}}^2} v_\xi \right],\ \xi_S < \xi < 1,\ 0 < t, \tag{A.5}$$

$$\text{B.C.:} \quad \begin{array}{l} v(\xi = \xi_S, t) = 0,\ 0 \le t, \\ v(\xi = 1^-, t) = T_{\text{Ice}} < 0,\ 0 \le t. \end{array} \tag{A.6}$$

Specialization to one-phase problem is omitted here. We remark that (i) the spatial boundary $\xi = 1$, which corresponds to infinity in model I, is a removable singularity here, and (ii) the interface point is related to that of the semi-infinite interval by

$$\xi_S = \frac{S(t) - x_{\text{ref}}}{S(t) + x_{\text{ref}}},$$

which depends on $\tau(= t)$ only.

Appendix B: Tables

Model	*Discretization*	*Coordinate*	*Grid*	*Spatial differentiation*
1a	FD-FD	fixed	static	implicit
1b	FD-FD	fixed	dynamic	implicit
1c	FD-FD	fixed	dynamic	explicit
1d	FD-FD	moving		explicit
2	FD-DM	fixed	dynamic	implicit

Table B.1: Numerical models

$Parameter-$ set	$Spatial-$ $range$	k_W k_W	k_I k_I	α α	T_{Water} T_{Water}	T_{Ice} T_{Ice}
first	$0 \leq x \leq 10$	5.5967e-02	2.0260e-01	1.0	1.0	-1.0
second	$0 \leq x \leq 6$	5.5967e-03	2.0260e-02	1.0	1.0	-1.0

Table B.2: Two sets of physical parameters

$parameter - set$	t_{end}	x_{max}	$analytic - solution$
first	12.0	2.0	-5.5760888305236378e-01
first	12.0	4.0	-9.1540961863156045e-01
first	12.0	6.0	-9.9209835612639885e-01
first	12.0	8.0	-9.9965322317623884e-01
first	12.0	10.0	-9.9999300606173236e-01
first	12.0	12.0	-9.9999993602806814e-01
first	12.0	14.0	-9.9999999973683862e-01
first	12.0	16.0	-9.9999999999951583e-01
first	12.0	18.0	-9.9999999999999956e-01
first	12.0	20.0	-1.0000000000000000e+00
second	12.0	2.0	-9.9479873343245229e-01
second	12.0	4.0	-9.9999998781166299e-01
second	12.0	6.0	-1.0000000000000000e-00

Table B.3: Dirichlet data towards infinity with two sets of parameters

Extrapolation Scheme	Grid	Sch	Δt	Δx	r_{max}	r_{av}	e_{max}	e_{av}	e_S
1	sta	im	1.0e-4	1.0e-2	5.9e-8	1.8e-10	2.5e-3	8.5e-5	4.3e-4
2	sta	im	1.0e-4	1.0e-2	5.3e-8	1.8e-10	4.4e-4	1.6e-5	7.7e-5
3	sta	im	1.0e-4	1.0e-2	5.4e-8	1.8e-10	8.0e-5	4.0e-6	-1.2e-5
5	sta	im	1.0e-4	1.0e-2					failed
6	sta	im	1.0e-4	1.0e-2	5.3e-8	1.8e-10	4.4e-4	1.6e-5	7.7e-5
7	sta	im	1.0e-4	1.0e-2	5.4e-8	1.8e-10	8.0e-5	4.0e-6	-1.2e-5
1	dyn	im	1.0e-4	1.0e-2	4.1e-6	1.5e-07	5.0e-3	1.7e-4	8.8e-4
2	dyn	im	1.0e-4	1.0e-2	4.1e-6	1.5e-07	6.8e-4	2.8e-5	1.2e-4
3	dyn	im	1.0e-4	1.0e-2	4.1e-6	1.5e-07	2.1e-4	6.7e-6	-2.8e-5
5	dyn	im	1.0e-4	1.0e-2	4.1e-6	1.5e-07	4.9e-3	1.7e-4	8.8e-4
6	dyn	im	1.0e-4	1.0e-2	4.1e-6	1.5e-07	6.6e-4	2.7e-5	1.2e-4
7	dyn	im	1.0e-4	1.0e-2	4.1e-6	1.5e-07	2.6e-4	8.4e-6	-3.7e-5
1	dyn	ex	1.0e-4	1.0e-2	4.1e-6	1.5e-07	4.9e-3	1.7e-4	8.7e-4
2	dyn	ex	1.0e-4	1.0e-2	4.1e-6	1.5e-07	7.4e-4	3.0e-5	1.3e-4
3	dyn	ex	1.0e-4	1.0e-2	4.1e-6	1.5e-07	1.1e-4	3.0e-6	-1.0e-5
5	dyn	ex	1.0e-4	1.0e-2	4.1e-6	1.5e-07	4.9e-3	1.7e-4	8.7e-4
6	dyn	ex	1.0e-4	1.0e-2	4.1e-6	1.5e-07	7.1e-4	2.9e-5	1.3e-4
7	dyn	ex	1.0e-4	1.0e-2	4.1e-6	1.5e-07	1.6e-4	4.7e-6	-1.9e-5

Table B.4: Effects of extrapolation schemes using second parameter set

G	Me	Sch	Δt	Δx	n_x	n_i	n_f	r_{max}	r_{av}	e_{max}	e_{av}	e_S	chk_S	$t1_{cpu}$	$t2_{cpu}$
st	FD	im	1.6e-3	4.0e-2	250	6	13	2.0e-5	9.8e-08	1.7e-4	1.9e-5	-5.6e-5	-6e-12	1	4
st	FD	im	4.0e-4	2.0e-2	500	11	25	2.2e-6	8.5e-09	3.5e-5	4.4e-6	-1.0e-5	-1e-13	9	28
st	FD	im	1.0e-4	1.0e-2	1000	20	49	3.3e-6	3.5e-09	7.8e-6	1.2e-6	-2.0e-6	1e-16	68	220
st	FD	im	2.5e-5	5.0e-3	2000	40	99	3.7e-7	2.2e-10	6.9e-6	5.3e-7	-4.3e-7	-5e-17	490	1689
dy	FD	im	1.6e-3	4.0e-2	250	6	13	6.9e-5	4.3e-06	4.2e-4	3.2e-5	-1.3e-4	1e-10	1	4
dy	FD	im	4.0e-4	2.0e-2	500	11	25	1.8e-5	1.1e-06	1.0e-4	7.3e-6	-3.0e-5	1e-12	13	33
dy	FD	im	1.0e-4	1.0e-2	1000	20	49	4.5e-6	2.7e-07	2.5e-5	1.9e-6	-6.2e-6	2e-13	102	252
dy	FD	im	2.5e-5	5.0e-3	2000	40	99	1.1e-6	6.8e-08	6.9e-6	7.0e-7	-1.5e-6	2e-15	758	1965
dy	FD	ex	1.6e-3	4.0e-2	250	6	13	6.3e-5	4.3e-06	9.0e-4	5.7e-5	5.9e-4	7e-11	1	3
dy	FD	ex	4.0e-4	2.0e-2	500	11	25	1.6e-5	1.1e-06	5.5e-4	3.5e-5	3.2e-4	1e-12	5	24
dy	FD	ex	1.0e-4	1.0e-2	1000	20	49	4.2e-6	2.7e-07	3.0e-4	1.9e-5	1.6e-4	1e-13	37	188
dy	FD	ex	2.5e-5	5.0e-3	2000	40	99	1.1e-6	6.8e-08	1.5e-4	1.0e-5	8.4e-5	1e-15	284	1470
dy	FD	mix-1	1.0e-4	1.0e-2	1000	20	49	4.5e-6	2.7e-07	3.4e-4	2.2e-5	-1.7e-4	3e-13	67	217
dy	FD	mix-2	1.0e-4	1.0e-2	1000	20	49	4.2e-6	2.7e-07	3.0e-4	1.9e-5	-1.6e-4	1e-13	24	175
mo	FD	ex	1.0e-4	5.0e-2	998	20	20	3.6e-6	3.3e-07	3.6e-2	4.9e-3	-9.2e-2	-1e-14	40	181
mo	FD	ex	5.0e-5	5.0e-2	998	20	20	1.8e-6	1.6e-07	3.6e-2	4.9e-3	-9.2e-2	-2e-15	80	360
mo	FD	ex	2.5e-5	2.5e-2	1995	40	40	9.2e-7	8.2e-08	3.6e-2	4.9e-3	-9.2e-2	-5e-16	309	1420
dy	DM	im	1.0e-3		300	7	15	1.4e-2	5.4e-05	9.7e-4	8.6e-5	-4.6e-4		1837	1843
dy	DM	im	1.0e-3		300	7	15	1.4e-2	5.4e-05	9.7e-4	8.6e-5	-4.6e-4		1723	1729

Table B.5: Semi-infinite interval models with first parameter set

G	Me	Sch	Δt	Δx	n_x	n_i	n_f	r_{max}	r_{av}	e_{max}	e_{av}	$e_{_S}$	$chk_{_S}$	$t1_{cpu}$	$t2_{cpu}$
st	FD	im	4.0e-4	2.0e-2	1000	10	24	2.2e-6	4.3e-09	3.5e-5	2.0e-6	-1.0e-5	-1e-13	17	51
st	FD	im	1.0e-4	1.0e-2	2000	20	49	3.3e-6	1.8e-09	7.8e-6	4.8e-7	-2.0e-6	1e-16	134	408
st	FD	im	2.5e-5	5.0e-3	4000	41	98	3.7e-7	1.1e-10	1.8e-6	1.1e-7	-4.3e-7	-5e-17	967	3139
dy	FD	im	4.0e-4	2.0e-2	1000	10	24	1.8e-5	5.7e-07	1.0e-4	3.5e-6	-2.9e-5	1e-12	25	60
dy	FD	im	1.0e-4	1.0e-2	2000	20	49	4.5e-6	1.4e-07	2.5e-5	8.3e-7	-6.1e-6	2e-13	202	477
dy	FD	im	2.5e-5	5.0e-3	4000	41	98	1.1e-6	3.6e-08	6.3e-6	2.0e-7	-1.5e-6	2e-15	2426	4644
dy	FD	ex	4.0e-4	2.0e-2	1000	10	24	1.6e-5	5.7e-07	5.5e-4	1.7e-5	3.2e-4	1e-12	9	44
dy	FD	ex	1.0e-4	1.0e-2	2000	20	49	4.2e-6	1.4e-07	3.0e-4	9.4e-6	1.6e-4	1e-13	73	343
dy	FD	ex	2.5e-5	5.0e-3	4000	41	98	1.1e-6	3.6e-08	1.5e-4	4.8e-6	8.4e-5	1e-15	1477	3673
mo	FD	ex	1.0e-4	5.0e-2	1994	20	20	3.6e-6	1.6e-07	3.6e-2	2.4e-3	-9.2e-2	-1e-14	54	310
mo	FD	ex	2.5e-5	2.5e-2	3989	40	40	9.2e-7	4.1e-08	3.6e-2	2.4e-3	-9.2e-2	-5e-16	1277	3362

Table B.6: First parameter set and $x_{max} = 20$

G	Me	Sch	Δt	Δx	n_x	n_i	n_f	r_{max}	r_{av}	e_{max}	e_{av}	$e_{_S}$	$chk_{_S}$	$t1_{cpu}$	$t2_{cpu}$
st	FD	im	4.0e-4	2.0e-2	300	3	7	4.9e-7	2.1e-09	4.0e-4	1.9e-5	-6.6e-5	-4e-13	3.7	14.5
st	FD	im	1.0e-4	1.0e-2	600	6	25	5.4e-8	1.8e-10	8.0e-5	4.0e-6	-1.2e-5	-7e-15	24.1	108.8
st	FD	im	2.5e-5	5.0e-3	1200	12	31	1.6e-7	1.4e-10	1.6e-5	8.7e-7	-2.5e-6	-2e-17	180.0	842.7
dy	FD	im	4.0e-4	2.0e-2	300	3	7	1.6e-5	5.8e-07	1.0e-3	3.4e-5	-1.5e-4	9e-13	6.1	17.0
dy	FD	im	1.0e-4	1.0e-2	600	6	15	4.1e-6	1.5e-07	2.1e-4	6.7e-6	-2.8e-5	5e-14	43.2	127.7
dy	FD	im	2.5e-5	5.0e-3	1200	12	31	1.1e-6	3.8e-08	4.8e-5	1.4e-6	-5.4e-6	2e-14	336.2	1004.2
dy	FD	ex	4.0e-4	2.0e-2	300	3	7	1.5e-5	5.8e-07	7.9e-4	2.5e-5	-1.1e-4	9e-13	3.2	14.2
dy	FD	ex	1.0e-4	1.0e-2	600	6	15	4.1e-6	1.5e-07	1.1e-4	3.0e-6	-1.0e-5	5e-14	22.8	107.3
dy	FD	ex	2.5e-5	5.0e-3	1200	12	31	1.0e-6	3.8e-08	7.5e-6	4.6e-7	3.3e-6	2e-14	183.9	861.4
mo	FD	ex	1.0e-3	1.0e-1	947	10	10	3.4e-5	1.7e-06	3.6e-2	2.5e-3	-2.9e-2	-5e-13	3.9	16.2
mo	FD	ex	5.0e-3	1.0e-1	947	10	10	1.7e-5	8.6e-07	3.6e-2	2.5e-3	-2.9e-2	-1e-13	7.7	32.2
mo	FD	ex	2.5e-3	1.0e-1	947	10	10	8.6e-6	4.3e-07	3.6e-2	2.5e-3	-2.9e-2	-2e-14	16.5	65.9
mo	FD	ex	2.5e-4	5.0e-2	1892	20	20	9.0e-6	4.3e-07	3.6e-2	2.6e-3	-2.9e-2	-2e-14	30.3	127.3
mo	FD	ex	1.0e-4	5.0e-2	1892	20	20	3.6e-6	1.7e-07	3.6e-2	2.6e-3	-2.9e-2	-3e-15	77.2	321.1
mo	FD	ex	5.0e-5	5.0e-2	1892	20	20	1.8e-6	8.7e-08	3.6e-2	2.6e-3	-2.9e-2	-7e-16	155.2	642.4

Table B.7: Semi-infinite interval models with second parameter set

G	Me	Sch	Δt	Δx	n_x	n_i	n_f	r_{max}	r_{av}	e_{max}	e_{av}	$e_{_S}$	$chk_{_S}$	$t1_{cpu}$	$t2_{cpu}$
st	FD	im	1.0e-4	1.0e-2	600	6	15	5.3e-8	1.8e-10	4.4e-4	1.6e-5	7.7e-5	1e-13	16.9	103.5
st	FD	im	2.5e-5	5.0e-3	1200	12	31	1.5e-7	1.3e-10	1.1e-4	4.0e-6	1.9e-5	1e-14	124.3	788.6
dy	FD	im	1.0e-4	1.0e-2	600	6	15	4.1e-6	1.5e-07	6.8e-4	2.8e-5	1.2e-4	4e-14	29.5	114.7
dy	FD	im	2.5e-5	5.0e-3	1200	12	31	1.1e-6	3.8e-08	1.8e-4	7.2e-6	3.3e-5	1e-14	220.3	883.2
dy	FD	ex	1.0e-4	1.0e-2	600	6	15	4.1e-6	1.5e-07	7.4e-4	3.0e-5	1.3e-4	4e-14	15.9	100.3
dy	FD	ex	2.5e-5	5.0e-3	1200	12	31	1.0e-6	3.8e-08	2.0e-4	8.0e-6	3.7e-5	1e-14	116.6	780.9

Table B.8: Second order extrapolation and second parameter set

Appendix C: Figures

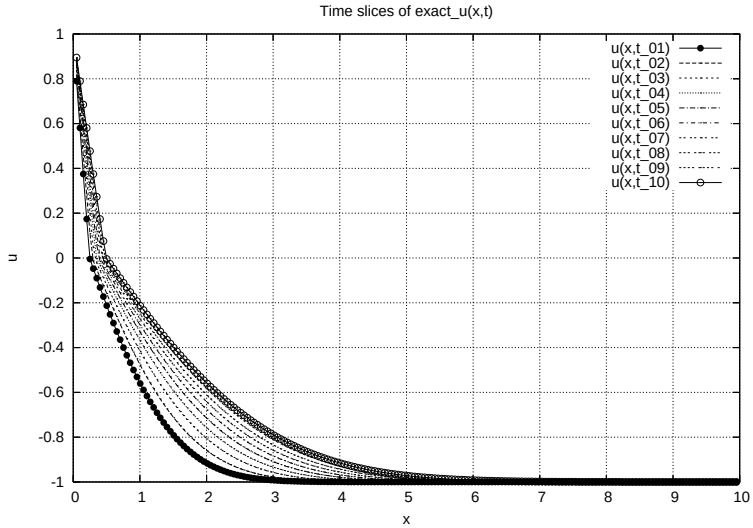

(a) u in semi-infinite interval

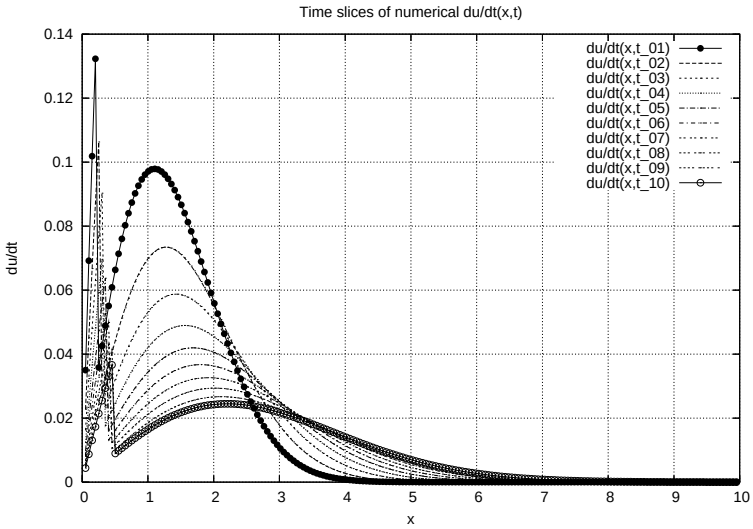

(b) du/dt in semi-infinite interval

Figure C.1: Analytic solution and temporal derivative at ten specific times

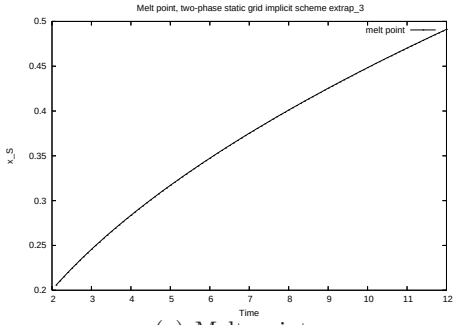

(a) Melt point

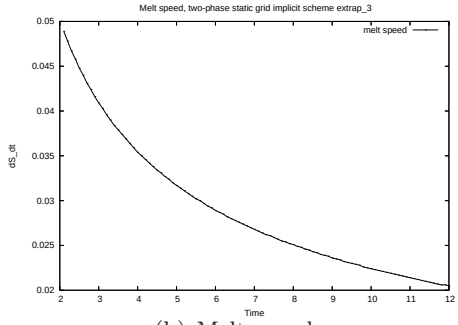

(b) Melt speed

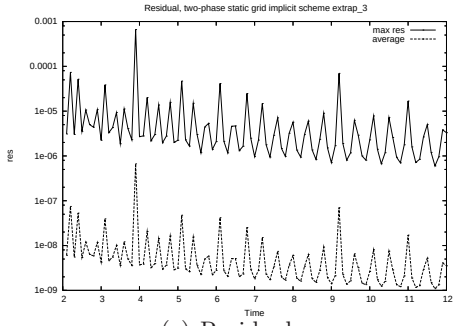

(c) Residuals

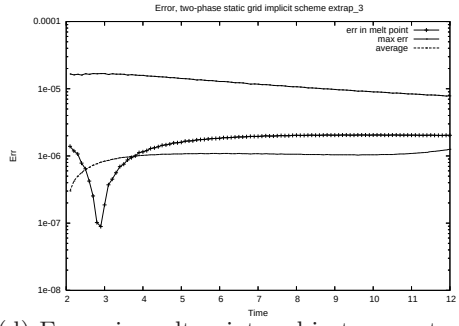

(d) Errors in melt point and in temperature

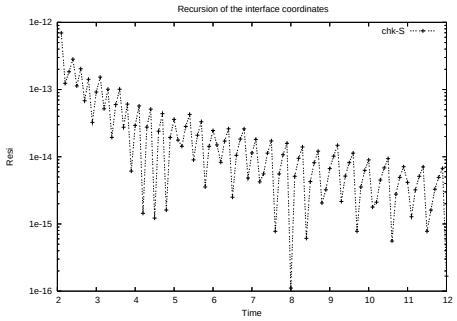

(e) Recursion of the interface

Figure C.2: Computation on static grid using first parameter set

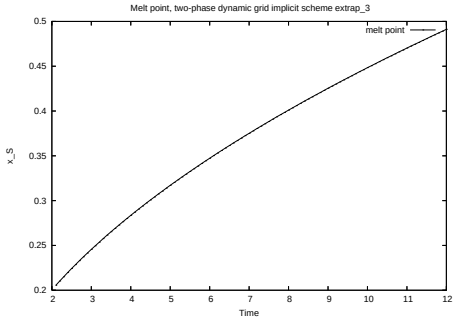

(a) Melt point

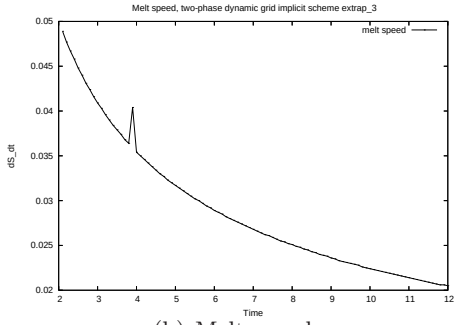

(b) Melt speed

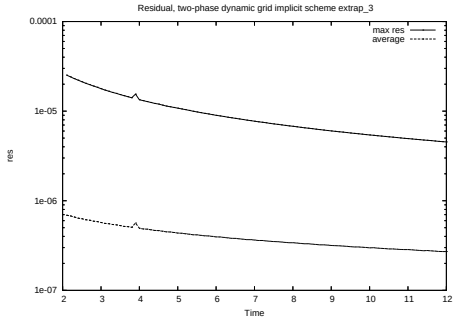

(c) Residuals

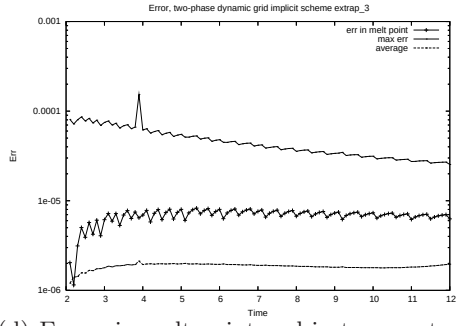

(d) Errors in melt point and in temperature

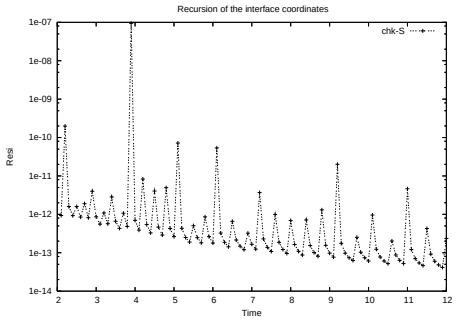

(e) Recursion of the interface

Figure C.3: Computation on dynamic grid using first parameter set

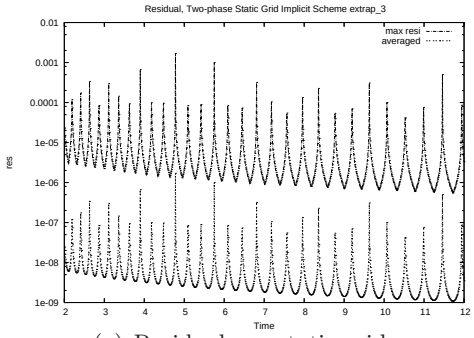

(a) Residuals on static grid

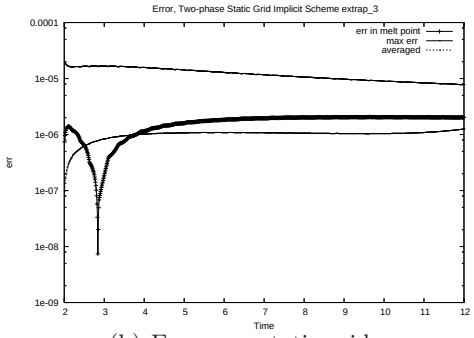

(b) Errors on static grid

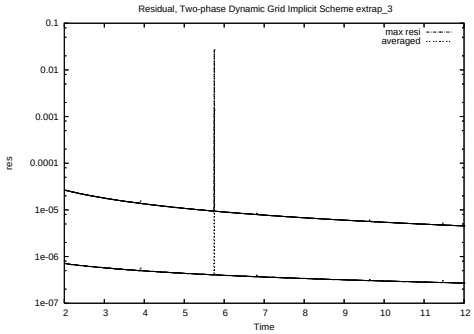

(c) Residuals on dynamic grid implicit

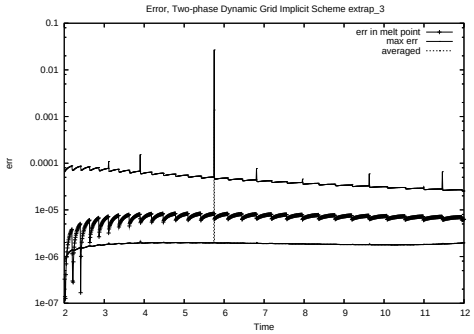

(d) Errors on dynamic grid implicit

Figure C.4: Accuracy of FD-FD using first parameter set

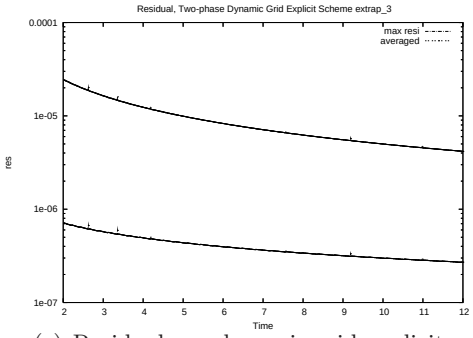

(e) Residuals on dynamic grid explicit

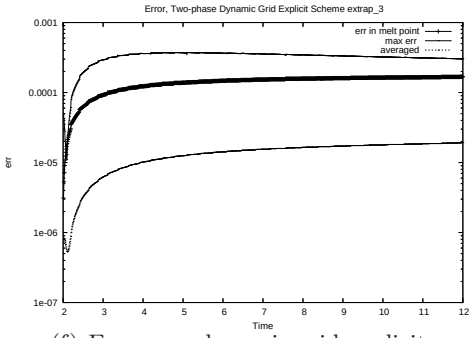

(f) Errors on dynamic grid explicit

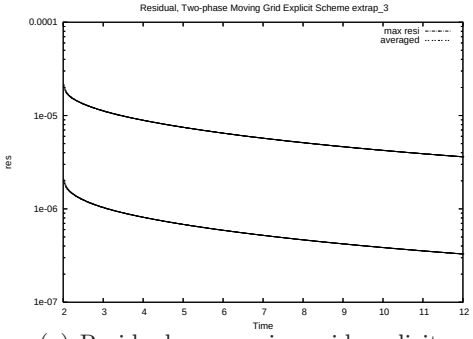

(g) Residuals on moving grid explicit

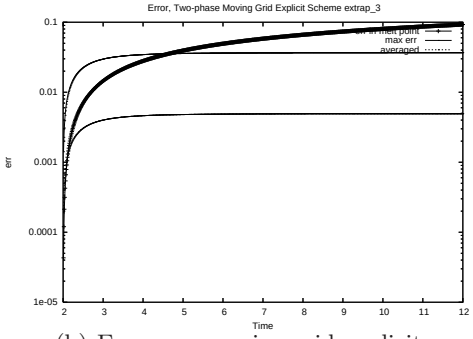

(h) Errors on moving grid explicit

Figure C.4: Continuation: Accuracy of FD-FD using first parameter set

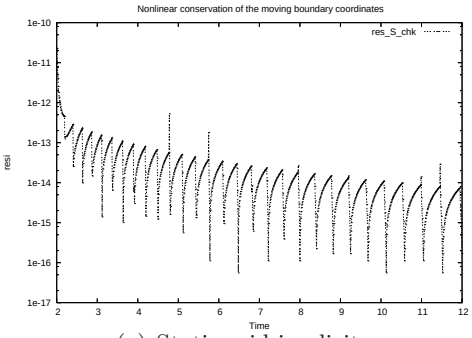

(a) Static grid implicit

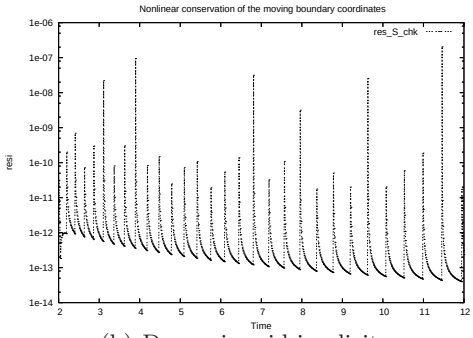

(b) Dynamic grid implicit

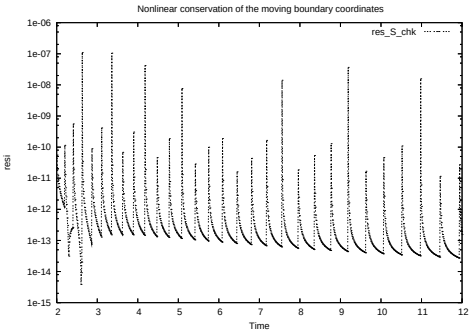

(c) Dynamic grid explicit

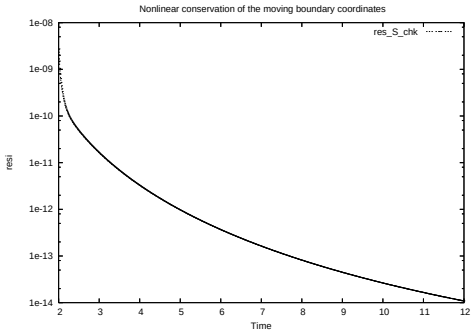

(d) Moving grid explicit

Figure C.5: Recursion for FD-FD using first parameter set

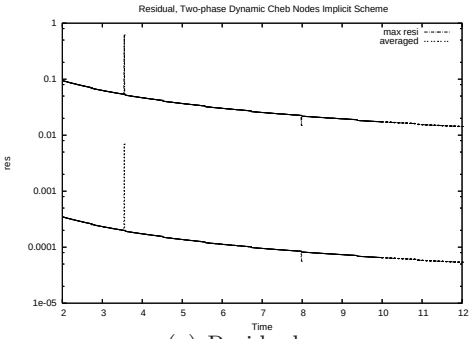

(a) Residuals

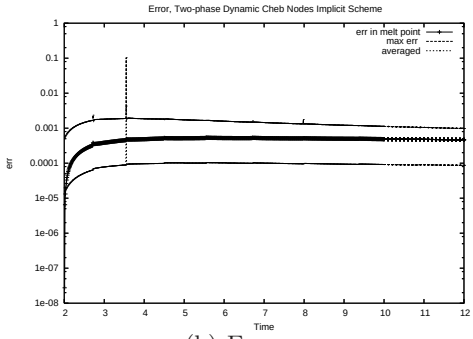

(b) Errors

Figure C.6: Accuracy of FD-DM using first parameter set

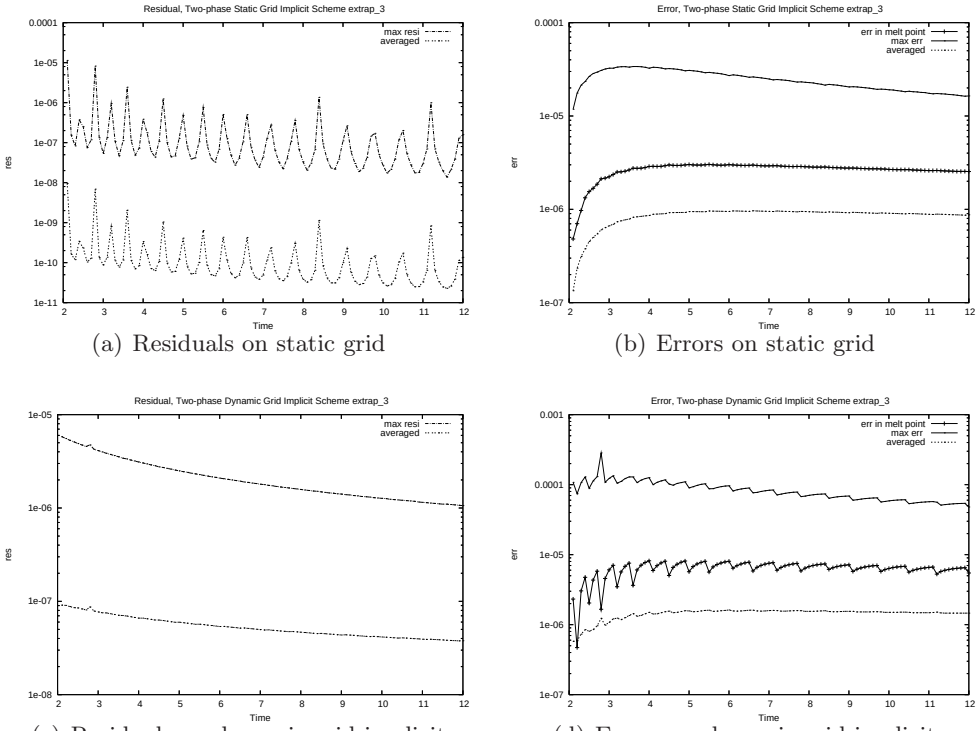

(a) Residuals on static grid

(b) Errors on static grid

(c) Residuals on dynamic grid implicit

(d) Errors on dynamic grid implicit

Figure C.7: Accuracy for FD-FD using second parameter set

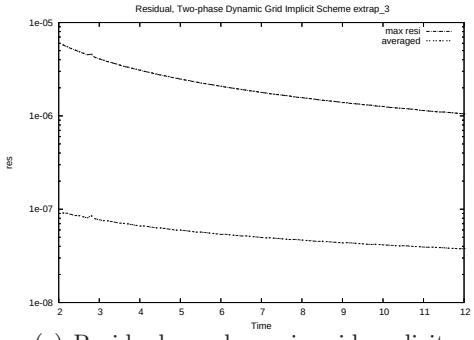

(e) Residuals on dynamic grid explicit

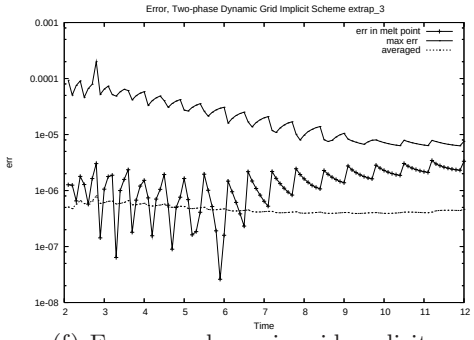

(f) Errors on dynamic grid explicit

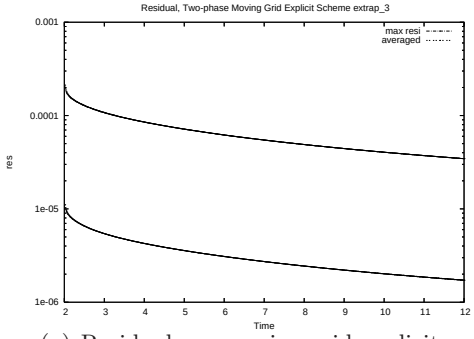

(g) Residuals on moving grid explicit

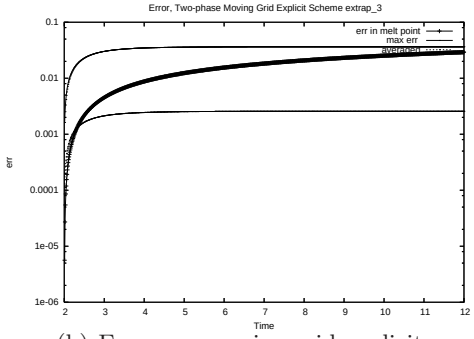

(h) Errors on moving grid explicit

Figure C.7: Continuation: Accuracy for FD-FD using second parameter set